Editors' Suggestion   Featured in Physics

Emergence of a Spin Microemulsion in Spin-Orbit Coupled Bose-Einstein Condensates

Ethan C. McGarrigle[1,*] Kris T. Delaney[2] Leon Balents[3,4] and Glenn H. Fredrickson[1,2,5,†]

[1]*Department of Chemical Engineering, University of California, Santa Barbara, California 93106, USA*
[2]*Materials Research Laboratory, University of California, Santa Barbara, California 93106, USA*
[3]*Kavli Institute for Theoretical Physics, University of California, Santa Barbara, California 93106, USA*
[4]*Canadian Institute for Advanced Research, Toronto, Ontario M5G 1M1, Canada*
[5]*Materials Department, University of California, Santa Barbara, California 93106, USA*

We report the first numerical prediction of a "spin microemulsion"—a phase with undulating spin domains resembling classical bicontinuous oil-water-surfactant emulsions—in two-dimensional systems of spinor Bose-Einstein condensates with isotropic Rashba spin-orbit coupling. Using field-theoretic numerical simulations, we investigated the melting of a low-temperature stripe phase with supersolid character and find that the stripes lose their superfluidity at elevated temperature and undergo a Kosterlitz-Thouless-like transition into a spin microemulsion. Momentum distribution calculations highlight a thermally broadened occupation of the Rashba circle of low-energy states with macroscopic and isotropic occupation around the ring. We provide a finite-temperature phase diagram that positions the emulsion as an intermediate, structured isotropic phase with residual quantum character before transitioning at higher temperature into a structureless normal fluid.

Introduction.—Microemulsion phases are typically found in synthetic soft matter systems [1–3], most prominently in oil-water-surfactant mixtures [4–6]. Two immiscible species form enriched domains while often a third minority component stabilizes their interfaces, playing the role of a surfactant or amphiphile. Another example is ternary polymer blends, where two incompatible homopolymers can form a bicontinuous microemulsion in the presence of a high-molecular-weight diblock copolymer [7,8]. Beyond the classical soft matter context, microemulsionlike phases are proposed as intermediates between Wigner crystals and Fermi liquids [9,10] in 2D electronic systems such as metal-oxide-semiconductor field-effect transistors [11–13].

A microemulsion analog phase is plausible for bosons with isotropic two-dimensional (2D) "Rashba" spin-orbit coupling (SOC). A continuous circle with radius q_0 of degenerate energy minima appears in the single-particle dispersion and constitutes a massive ground-state degeneracy, analogous to 2D Rashba electronic systems [14–16]. The circular degeneracy provides a setting where isotropic density modulations with dominant length scale $2\pi/q_0$ can produce an isotropic, emulsionlike phase.

Although most experimental realizations of SOC in cold atom systems access anisotropic or one-dimensional SOC [17–22], a recent experiment from the NIST group [23] achieved a Rashba-like 2D SOC, but did not quite achieve a circular single-particle degeneracy. Exotic behavior has been speculated: that Rashba bosons could host a Bose metal or Rashba Luttinger liquid [24], exhibit fractional Hall-like states [23], or undergo a statistical transmutation into composite fermions [25]. Bogoliubov theory, mean-field theory, and semiclassical numerical simulations [26–31] provide mounting evidence that bulk systems of Rashba bosons will produce a plane-wave or stripe ground state near $T = 0$, where Bose condensation occurs into one or two minima at nonzero momenta, respectively. However, their finite temperature physics has eluded conclusive theoretical understanding due to a sign problem inherent to the SOC Hamiltonian.

In this Letter, we interrogate a second-quantized model of interacting, pseudospin-1/2 Rashba bosons at finite temperature using an approximation-free, field-theoretic simulation technique that overcomes the sign problem. Our investigation reveals a novel microemulsion phase with undulating pseudospin domains reflecting an isotropic occupation of the Rashba circle of low-energy states. We perform simulations at several SOC strengths and temperatures to compute a phase diagram and confirm the microemulsion's existence between a low-temperature superfluid spin-stripe phase and a high-temperature paramagnetic, normal fluid.

Methods.—We incorporate 2D isotropic SOC into a model of interacting pseudospin-1/2 bosons via a uniform and time-independent non-Abelian gauge potential $\mathcal{A} = \hbar\kappa(\underline{\sigma}^x, \underline{\sigma}^y)$ [32], where $\underline{\sigma}^\nu$ are the spin-1/2 Pauli matrices in the ν direction and κ is the SOC strength. Assemblies of interacting pseudospin-1/2 bosons in 2D are well described by the second-quantized Hamiltonian:

$$\hat{H} = \sum_{\alpha\gamma} \int d^2r\, \hat{\psi}_\alpha^\dagger(\mathbf{r}) \left[\frac{1}{2m}(\hat{\mathbf{p}}\,\underline{I} - \mathcal{A})^2 - \mu\underline{I} \right]_{\alpha\gamma} \hat{\psi}_\gamma(\mathbf{r})$$
$$+ \frac{1}{2}\sum_{\alpha\gamma} \int d^2r\, \hat{\psi}_\alpha^\dagger(\mathbf{r})\hat{\psi}_\gamma^\dagger(\mathbf{r})(g_0\underline{I} + g_1\underline{\sigma}^x)_{\alpha\gamma}\hat{\psi}_\alpha(\mathbf{r})\hat{\psi}_\gamma(\mathbf{r}),$$

$$(1)$$

where $\hat{\psi}_\alpha(\mathbf{r})$ is a second-quantized field operator for pseudospin species α obeying Bose commutation relations [33], $\hat{\mathbf{p}} = -i\hbar\nabla$ is the canonical momentum operator, $\underline{I}$ is the 2×2 identity matrix for pseudospin indices, μ is chemical potential, and m is the atomic mass shared by both pseudospin species. We assume contact pairwise interactions where the repulsive coupling constants g_0 and g_1 are parametrized by s-wave scattering lengths $a_{s,0}$ and $a_{s,1}$ for like and unlike pseudospin scattering events, respectively, and correspond to a symmetric matrix of coupling constants.

We define a natural length scale $\ell = \sqrt{(\hbar^2/2m\mu_{\text{eff}})}$ and energy scale μ_{eff}, where μ_{eff} is an effective chemical potential that incorporates the SOC recoil energy $\mu_{\text{eff}} \equiv \mu - \hbar^2\kappa^2/m$. After rescaling all field operators, spatial derivatives, and integrals using ℓ and μ_{eff}, we identify four dimensionless quantities that govern the model's universal behavior: a repulsion scale $\tilde{g} \equiv 2mg_0/\hbar^2$, a SOC strength $\tilde{\kappa} \equiv \kappa\ell$, a temperature $\tilde{T} \equiv k_BT/\mu_{\text{eff}}$, and a miscibility parameter $\eta_g \equiv g_1/g_0$. For this study, we confine our simulations to slightly immiscible conditions $\eta_g = 1.1 > 1$, which promote a stripe ground state at low temperatures.

To access finite temperature, we use Feynman's imaginary time path integral approach to convert the many-boson problem into a coherent state quantum field theory in the grand canonical ensemble [34]. The degrees of freedom are a complex conjugate pair of bosonic coherent state fields $\phi_\alpha(\mathbf{r}, \tau)$, $\phi_\alpha^*(\mathbf{r}, \tau)$ for each pseudospin species, obeying periodic boundary conditions in imaginary time τ. The resulting grand partition function $\mathcal{Z} = \int \mathcal{D}(\boldsymbol{\phi}, \boldsymbol{\phi}^*)e^{-S[\boldsymbol{\phi},\boldsymbol{\phi}^*]}$ consists of functional integrals over the real and imaginary parts of the field components at each space-imaginary time point; $\boldsymbol{\phi}$ and $\boldsymbol{\phi}^*$ are two-component vectors in the pseudospin species. A configuration's statistical weight is described by e^{-S}, where $S[\boldsymbol{\phi}, \boldsymbol{\phi}^*]$ is a complex-valued action functional that presents a numerically foreboding sign problem:

$$S[\boldsymbol{\phi}, \boldsymbol{\phi}^*] = \sum_\alpha \sum_{j=0}^{N_\tau-1} \int d^2r\, \phi_{\alpha,j}^*(\mathbf{r})[\phi_{\alpha,j}(\mathbf{r}) - \phi_{\alpha,j-1}(\mathbf{r})]$$
$$+ \frac{\tilde{\beta}}{N_\tau}\sum_{\alpha,\gamma}\sum_{j=0}^{N_\tau-1} \int d^2r\, \phi_{\alpha,j}^*(\mathbf{r})\hat{\mathcal{K}}_{\alpha,\gamma}\phi_{\gamma,j-1}(\mathbf{r})$$
$$+ \frac{\tilde{\beta}\tilde{g}}{2N_\tau}\sum_{\alpha,\gamma}\sum_{j=0}^{N_\tau-1} \int d^2r\, \phi_{\alpha,j}^*(\mathbf{r})$$
$$\times \phi_{\gamma,j}^*(\mathbf{r})(\underline{I} + \eta_g\underline{\sigma}^x)_{\alpha\gamma}\phi_{\gamma,j-1}(\mathbf{r})\phi_{\alpha,j-1}(\mathbf{r}), \quad (2)$$

where $\tilde{\beta} = 1/\tilde{T}$, imaginary time $\tau \in [0, \tilde{\beta}]$ has been discretized into N_τ points, and the index j labels the imaginary-time slice. We enforce periodic boundary conditions in imaginary time, e.g., $\phi_{\alpha,0}(\mathbf{r}) = \phi_{\alpha,N_\tau}(\mathbf{r})$, as well as in the two spatial dimensions. $\hat{\underline{\mathcal{K}}}$ is a Hermitian one-body matrix with equal diagonal entries $\hat{\mathcal{K}}_{\uparrow\uparrow} = \hat{\mathcal{K}}_{\downarrow\downarrow} = -\tilde{\nabla}^2 - 1$, and $\hat{\mathcal{K}}_{\uparrow\downarrow} = \hat{\mathcal{K}}_{\downarrow\uparrow}^\dagger = -2\tilde{\kappa}[-i\partial_{\tilde{x}} - \partial_{\tilde{y}}]$, where $\partial_{\tilde{x}}$ and $\tilde{\nabla}^2$ indicate a dimensionless spatial derivative and Laplacian, respectively. $\mathbf{r}$ is a dimensionless coordinate.

In our field-theoretic simulation method, we discretize the coherent state fields in the three space-imaginary time dimensions and numerically sample the field elements by evolving the complex Langevin algorithm [35]

$$\frac{\partial}{\partial t}\phi_{\alpha,j}(\mathbf{r}, t) = -\frac{\delta S[\phi, \phi^*]}{\delta\phi_{\alpha,j}^*(\mathbf{r}, t)} + \eta_{\alpha,j}(\mathbf{r}, t)$$
$$\frac{\partial}{\partial t}\phi_{\alpha,j}^*(\mathbf{r}, t) = -\frac{\delta S[\phi, \phi^*]}{\delta\phi_{\alpha,j}(\mathbf{r}, t)} + \eta_{\alpha,j}^*(\mathbf{r}, t), \quad (3)$$

forward in fictitious time t using an exponential time-differencing integrator [36]. $\eta_{\alpha,j} = \eta_{\alpha,j}^{(1)} + i\eta_{\alpha,j}^{(2)}$ and $\eta_{\alpha,j}^* = \eta_{\alpha,j}^{(1)} - i\eta_{\alpha,j}^{(2)}$ are complex conjugate white noise sources that are built from real noise fields $\eta_{\alpha,j}^{(1)}$ and $\eta_{\alpha,j}^{(2)}$ with $\langle\eta_{\alpha,j}^{(\mu)}(\mathbf{r}, t)\rangle = 0$ and $\langle\eta_{\alpha,j}^{(\mu)}(\mathbf{r}, t)\eta_{\beta,k}^{(\nu)}(\mathbf{r}', t')\rangle = \delta_{\mu,\nu}\delta_{\alpha,\beta}\delta_{j,k} \times \delta(\mathbf{r} - \mathbf{r}')\delta(t - t')$. Our pseudospectral implementation assumes periodic boundary conditions in all dimensions. Observables of interest such as the pressure and internal energy are obtained by averaging field operators (functionals of the coherent state fields) over fictitious complex-Langevin time trajectories. This procedure overcomes the statistical weight's highly oscillatory nature and provides bias-free thermodynamic properties at finite temperature [37,38].

To identify the equilibrium phase, we calculated snapshots of the resulting structure's real-space density profile as well as thermal averages (via fictitious Langevin time averages) of the momentum state distribution in $\mathbf{k}$ space, where $\mathbf{k} = 2\pi(n_x/L_x, n_y/L_y)$ is the discrete wave vector labelling momentum states with $n \in \mathbb{Z}$. The density profile for pseudospin species α and the momentum distribution were calculated via $\rho_\alpha[\boldsymbol{\phi}, \boldsymbol{\phi}^*; \mathbf{r}] = 1/N_\tau\sum_{j=0}^{N_\tau-1}\phi_{\alpha,j}^*(\mathbf{r})\phi_{\alpha,j-1}(\mathbf{r})$ and $N[\boldsymbol{\phi}, \boldsymbol{\phi}^*; \mathbf{k}] = A/N_\tau\sum_\alpha\sum_{j=0}^{N_\tau-1}\tilde{\phi}_{\alpha,j,-\mathbf{k}}^*\tilde{\phi}_{\alpha,j-1,\mathbf{k}}$, where $\tilde{\phi}$ refers to the Discrete Fourier Transform of ϕ, accessed numerically via Fast Fourier Transform algorithms [35], and $A = L_xL_y$ is the system size (area).

Appearance of a microemulsion.—At low temperatures and immiscible conditions ($\eta_g > 1$), the system possesses a stripe ground state with broken continuous translational and rotational symmetries, shown in Fig. 1(a). The stripe phase is a pseudospin density wave in one direction that resembles spin density waves found in electronic systems [13].
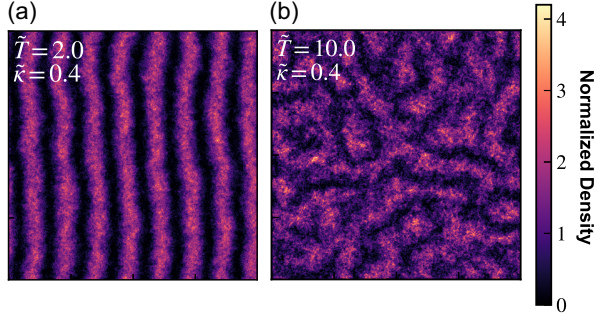
FIG. 1. Density profiles $\rho_\uparrow(\mathbf{r})$ of pseudospin bosons in the $|\uparrow\rangle$ state at $\tilde{\kappa} = 0.4$ and interaction conditions $\tilde{g} = 0.05$, and $\eta_g = 1.1$. (a), (b) The stripe phase with Rashba SOC transitions into an isotropic spin microemulsion above $\tilde{T}_c$. Profiles are snapshots normalized by the spatially averaged density.

However, in the presence of isotropic SOC and above a critical temperature, the spin stripes undulate and twist into an isotropic "spin emulsion" structure that resembles bicontinuous microemulsions found in soft matter systems [Fig. 1(b)]. Figure 1 qualitatively shows this transition from a quasi-long-range ordered stripe phase to an isotropic spin microemulsion via $|\uparrow\rangle$ density snapshots at different temperatures. Figure 2(a) provides a wide field of view of a larger microemulsion system with no quasi-long-range orientational order.

The momentum distribution is shown in Fig. 2(b) and highlights the isotropic character of the structured emulsion phase with characteristic domain width $\pi/2\tilde{\kappa}$. The significant occupation of momentum states with wave vector $|\mathbf{k}| = \tilde{\kappa}$ in Fig. 2(b) suggests a massive fragmentation of the quasicondensate onto the Rashba dispersion's circular manifold of states. This circular momentum distribution presents an appealing experimental signature for the microemulsion phase and could be observed in a time-of-flight cold atom experiment, using either spin-resolved (Stern-Gerlach) or spin-unresolved techniques.
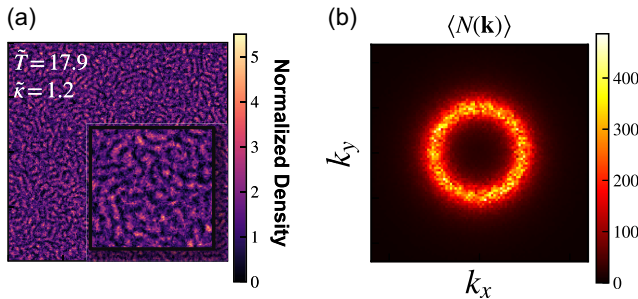

FIG. 2. A spin microemulsion phase with $\langle N \rangle \sim 4.8 \times 10^5$ particles at $\tilde{T} = 17.9$, $\tilde{\kappa} = 1.2$, $\tilde{g} = 0.05$, and $\eta_g = 1.1$. (a) Density profile $\rho_\uparrow(\mathbf{r})$ of pseudospin bosons in the $|\uparrow\rangle$ basis state, normalized by the spatially averaged density. A highlighted section is enlarged to show the local emulsionlike structure. (b) Thermal average momentum state occupation $N(\mathbf{k})$.

To study the local pseudospin details, we calculate components of the local magnetization field via $M_\nu[\boldsymbol{\phi}, \boldsymbol{\phi}^*; \mathbf{r}] = (1/N_\tau) \sum_{\alpha\beta} \sum_{j=0}^{N_\tau - 1} \phi_{\alpha,j}^*(\mathbf{r}) \sigma_{\alpha\beta}^\nu \phi_{\beta, j-1}(\mathbf{r})$, where $\sigma_{\alpha\beta}^\nu$ represents an element of the spin-1/2 Pauli matrix in the ν direction. Both the stripe and microemulsion phases are characterized by strong $M_z(\mathbf{r})$ domains shown in the color intensity of Fig. 3. Furthermore, the stripe and emulsion phase exhibit rich $M_x(\mathbf{r})$ and $M_y(\mathbf{r})$ planar pseudospin textures. The close-up regions in Figs. 3(a) and 3(b) highlight planar pseudospin defects present throughout both phases. The stripe phase hosts stable domain walls and 1D skyrmions commensurate with the stripe periodicity; however, thermal fluctuations induce pairs of oppositely charged planar pseudospin vortices between adjacent stripes [Fig. 3(a)]; in contrast, vortices in the microemulsion phase appear free and manifest as 2D skyrmions [Fig. 3(b)]. The shift from bound to free vortices across the stripe to microemulsion transition suggests a Kosterlitz-Thouless picture. These vortices in pseudospin disappear completely upon crossing over at higher temperatures to the paramagnetic normal fluid.

Phase transitions.—The predicted finite-temperature phase diagram in the $\tilde{T}$-$\tilde{\kappa}$ plane is shown in Fig. 4 for slightly immiscible and isotropic SOC conditions. To observe various thermal transitions, we varied the temperature at fixed $\tilde{\kappa} \geq 0.1$ and monitored the thermal-averaged momentum distributions, which revealed three distinct phases, shown in Figs. 5(a)–5(c). Different interaction strengths $\tilde{g} > 0$ and miscibility values $\eta_g > 1$ would shift
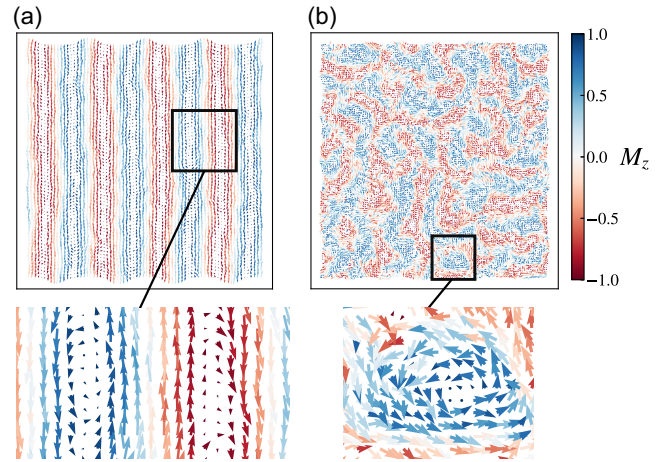

FIG. 3. Pseudospin textures and topological defects visualized via $\mathbf{M}(\mathbf{r})$ at $\tilde{\kappa} = 0.4$, $\tilde{g} = 0.05$, and $\eta_g = 1.1$ in (a) the stripe phase, $\tilde{T} = 1.1$, and (b) the microemulsion phase, $\tilde{T} = 10.25$. The color bar shows the magnitude of $M_z(\mathbf{r})$. Arrows represent the planar vector $[M_x(\mathbf{r}), M_y(\mathbf{r})]$. Boxed regions are enlarged to show planar pseudospin domain walls and vortices for the stripe and microemulsion phases, respectively. The plotted local magnetization vector is normalized by the local magnitude $|M(\mathbf{r})| = \sqrt{M_x^2(\mathbf{r}) + M_y^2(\mathbf{r}) + M_z^2(\mathbf{r})}$.
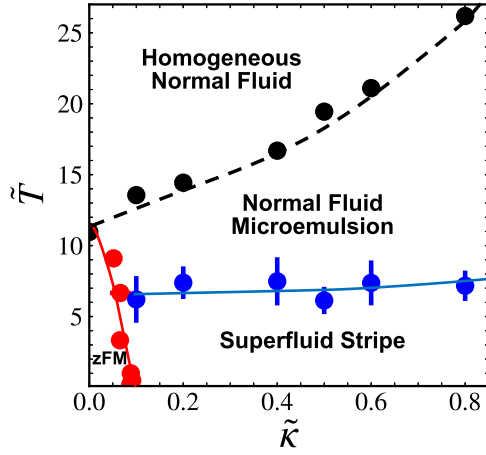
FIG. 4. Finite-temperature phase diagram in the $\tilde{T}$-$\tilde{\kappa}$ plane of interacting bosons with isotropic SOC in two dimensions, constructed for $\eta_g = 1.1$, $\tilde{g} = 0.05$. Lines are a guide for the eye, and error bars are discussed in Supplemental Material [39] [see also Refs. [40–42] therein]. The blue solid line denotes the Kosterlitz-Thouless-like critical transition, while the red line denotes a first order phase transition into the $\hat{z}$-ferromagnet (zFM) phase. The black dashed line depicts a crossover between the spin microemulsion and homogeneous normal fluid.

FIG. 5. Finite-temperature phase transitions at $\tilde{\kappa} = 0.5$, $\tilde{g} = 0.05$, and $\eta_g = 1.1$. (a)–(c) Momentum distribution $N(\mathbf{k})$ for the (a) stripe phase at $\tilde{T} = 3.3$, (b) spin microemulsion phase at $\tilde{T} = 13.2$, and (c) homogeneous normal fluid at $\tilde{T} = 40.0$. (d) Superfluid stiffness tensor across the stripe to emulsion thermal phase transition at various system sizes. The ρ_{SF}^{xx} (ρ_{SF}^{yy}) fraction is shown with blue (red) markers. (e) Isothermal compressibility at different system sizes, scaled for data collapse. The universal peak near $\tilde{T} = 19.4$ (gray shading) highlights the crossover from a structured microemulsion to a homogeneous normal fluid. All error bars are standard errors of the mean calculated during the Langevin time sample averaging process.

phase boundaries while leaving the topology of the phase diagram unaltered. The microemulsion emerges as a clear and robust intermediate between the low-temperature ordered stripe superfluid and a high-temperature homogeneous normal fluid.

Remarkably, the microemulsion's appearance at moderate $\tilde{T}$ coincides with a complete loss of superfluidity [Fig. 5(d)] from the stripe phase, showing characteristics similar to a Kosterlitz-Thouless transition. To determine that phase boundary for a given $\tilde{\kappa}$, the superfluid stiffness tensor's diagonal normal component ρ_{SF}^{xx} was tracked with increasing temperature for $\hat{x}$-modulated stripe phases. The superfluid density tensor is estimated using the phase twist method [43] $\rho_{SF}^{\mu\nu} = (m/\hbar^2 A)[\partial^2 \Omega(\mathbf{q})/\partial q_\mu \partial q_\nu]|_{\mathbf{q}\to 0}$, where $\Omega(\mathbf{q})$ is the thermodynamic grand potential after an imposed superflow proportional to $\mathbf{q}$, incorporated via a pseudospin and τ-independent phase shift to each coherent state field via $\phi_\alpha(\mathbf{r}, \tau) \to \phi_\alpha(\mathbf{r}, \tau)e^{i\mathbf{q}\cdot\mathbf{r}}$. The field operator functional used to calculate $\rho_{SF}^{\mu\nu}$ is detailed in Supplemental Material [39]. Using our dimensionless framework and superfluid density calculations, we estimate the stripe-microemulsion transition temperature in ^{87}Rb condensates to be near 150 nK, assuming a mixture of $|F = 1, m_F = \pm 1\rangle$ hyperfine states with an effective chemical potential of $\mu_{\text{eff}} = h \times 0.95$ kHz [44].

For vertically oriented stripes under isotropic SOC, the stripe phase is nearly pure superfluid in $\hat{x}$ but significantly normal fluid in $\hat{y}$; free particlelike excitations appear in the $\hat{y}$ Bogoliubov spectrum [26] and disrupt superfluidity along the stripes. In contrast, the $\hat{x}$ excitation spectrum [26] hosts double gapless bands that signify supersolid character
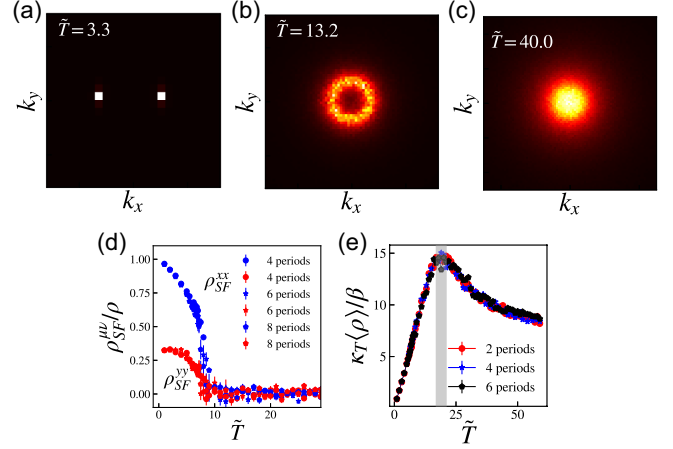
normal to the stripes and arise from the simultaneously broken $U(1)$ and continuous translational symmetries.

ρ_{SF}^{xx} declines to zero near the critical stripe melting temperature [Fig. 5(d)], reminiscent of the finite-size Kosterlitz-Thouless transition in conventional 2D superfluids, liquid crystals, and superconductors [45]. To determine the precise critical temperature, we conducted a finite-size scaling analysis in Supplemental Material [39] on ρ_{SF}^{xx}/ρ to correct for finite-size errors and estimate the Kosterlitz-Thouless transition temperature $\tilde{T}_c$ in the thermodynamic limit. The normal component ρ_{SF}^{xx}/ρ fraction experiences a full variation and serves as a more appropriate measure than ρ_{SF}/ρ of the helicity or superfluidity modulus for quantifying a universal jump. Despite the stripe's apparent smectic character observed in a modest simulation cell, the finite-temperature stripe phase in the thermodynamic limit should lose long range positional order in the presence of quantum and thermal fluctuations to produce a 2D superfluid nematic [29], analogous to the phonon and defect-mediated smectic to nematic transition in classical 2D liquid crystals [46,47]. Therefore, we expect that the observed transition would be a Kosterlitz-Thouless transition between a superfluid nematic and the normal fluid microemulsion in the thermodynamic limit. Our finite-size analysis suggests a transition mediated by the unbinding of half-vortex phase defects in the nematic superfluid, where the magnitude of the universal jump is modified [29].

At higher temperatures, the spin microemulsion continuously crosses over to a disordered paramagnetic state. On the single-particle level, this crossover overcomes an energy difference $\Delta \sim \tilde{\kappa}^2$ between the upper helicity branch and the degenerate circle on the lower helicity branch of the Rashba dispersion; this scaling supports the positive curvature of the microemulsion to homogeneous fluid crossover curve observed (Fig. 4). The homogeneous fluid represents a significant occupation of the single-particle branch with positive helicity and is supported by the momentum distribution in Figs. 5(b) and 5(c), where the maximum occupation moves from $|\mathbf{k}| = \tilde{\kappa}$ to $\mathbf{k} = \mathbf{0}$ as $\tilde{T}$ increases. This crossover coincides with an anomaly in the 2D isothermal compressibility $\kappa_T = -(1/A) \times (dA/dP)|_T$ [Fig. 5(e)] that shows no statistically significant finite-size error, suggesting a crossover rather than a critical phase transition with diverging correlation length. The field operator functional used to calculate κ_T is detailed in Supplemental Material [39].

At low SOC strength $\tilde{\kappa} < 0.1$ and low $\tilde{T}$, the system reduces to a weakly interacting pseudospin-1/2 Bose gas, where the immiscibility promotes a $\hat{z}$-ferromagnet (zFM) superfluid ground state with broken $\mathbb{Z}_2$ and $U(1)$ symmetries. This state is conveniently probed in the grand canonical ensemble where the system selects a nearly full occupation of either pseudospin state $|\uparrow\rangle$ or $|\downarrow\rangle$ due to a thermodynamic phase coexistence of two homogeneous superfluids with opposing macroscopic pseudospin. The transition between the zFM and the stripe phase was studied via direct calculation of the grand potential Ω for each phase [48], where the phase with the lowest grand potential is deemed more thermodynamically stable. Supplemental Material [39] includes observed jumps in order parameters such as the $\mathbf{k} = \mathbf{0}$ occupation fraction $N_{k=0}/N$ and the integrated $\hat{z}$ projection of the magnetization $M_z = \int d^2 r M_z(\mathbf{r})$, which suggest that the phase transition is first order and is confirmed by an observed kink in the grand potential at $\tilde{\kappa}_c$.

Conclusions.—We have discovered an isotropic spin microemulsion phase, found in Rashba spin-orbit coupled, Bose-Einstein condensates at finite temperature. Our Letter details its density profile, pseudospin profile, and momentum distribution, computed using complex Langevin sampling of a representative coherent state field theory. The microemulsion exhibits short-range correlations in z-pseudospin magnetization on a length scale $\ell \sim \pi/\tilde{\kappa}$, consistent with the Rashba circle of degenerate single-particle states at momentum $|\mathbf{k}| = \tilde{\kappa}$. This circular momentum distribution is reminiscent of other intermediate isotropic phases in condensed matter physics, such as the melting of Dzyaloshinskii-Moriya three-dimensional helimagnets [49] and itinerant magnets [50]. We quantify the superfluid fraction and find that the microemulsion is entirely normal fluid; however, the robust spinor domains

highlight the microemulsion's quantum character despite losing quasi-long-range translational and orientational order.

This work demonstrates the first appearance of an isotropic intermediate upon melting of a bosonic stripe phase and contributes to the growing literature on Bose liquid crystal analogs [51–53]. The data presented here suggest that the stripe-emulsion transition fits well into the broader context of a Kosterlitz-Thouless transition mediated by unbinding topological defects in 2D [46,47]; however, the finite-temperature transition is complicated by the presence of simultaneous dislocation defects in the stripe patterns, planar pseudospin vortices, and vortices in the superfluid phase. The precise interplay and role of each defect in the KT-like transition is a subject for future study.

This Letter provides insight into long-standing questions regarding the finite-temperature behavior of Rashba bosons and provides an explicit example of severely fragmented (quasi)condensation in a circular flat band, where the number of degenerate single-particle states is greater than the number of atoms in the system [54]. In this case, a singly condensed momentum state is absent and instead a spin-correlated, structured normal fluid phase emerges with a circular manifold of occupied momentum modes. This first computational prediction of an emulsion phase in cold atom systems serves to highlight a confluence among seemingly disparate fields—soft matter physics, electronic condensed matter physics, and atomic physics.

[*]emcgarrigle@ucsb.edu
[†]ghf@ucsb.edu

[1] D. D. Lee, S. H. Chen, C. F. Majkrzak, and S. K. Satija, Bulk and surface correlations in a microemulsion, Phys. Rev. E **52**, R29 (1995).

[2] S. Guo, H. Tao, G. Gao, S. Mhatre, Y. Lu, A. Takagi, J. Li, L. Mo, O. J. Rojas, and G. Chu, All-aqueous bicontinuous structured liquid crystal emulsion through intraphase

trapping of cellulose nanoparticles, Biomacromolecules **24,** 367 (2023).

[3] F. Bonelli, L. N. Carenza, G. Gonnella, D. Marenduzzo, E. Orlandini, and A. Tiribocchi, Lamellar ordering, droplet formation and phase inversion in exotic active emulsions, Sci. Rep. **9,** 2801 (2019).

[4] C. Huang, J. Forth, W. Wang, K. Hong, G. S. Smith, B. A. Helms, and T. P. Russell, Bicontinuous structured liquids with sub-micrometre domains using nanoparticle surfactants, Nat. Nanotechnol. **12,** 1060 (2017).

[5] P. G. De Gennes and C. Taupin, Microemulsions and the flexibility of oil/water interfaces, J. Phys. Chem. **86,** 2294 (1982).

[6] M. Clausse, J. Peyrelasse, J. Heil, C. Boned, and B. Lagourette, Bicontinuous structure zones in microemulsions, Nature (London) **293,** 636 (1981).

[7] F. S. Bates, W. W. Maurer, P. M. Lipic, M. A. Hillmyer, K. Almdal, K. Mortensen, G. H. Fredrickson, and T. P. Lodge, Polymeric Bicontinuous Microemulsions, Phys. Rev. Lett. **79,** 849 (1997).

[8] R. K. W. Spencer and M. W. Matsen, Coexistence of polymeric microemulsion with homopolymer-rich phases, Macromolecules **54,** 1329 (2021).

[9] B. Spivak and S. A. Kivelson, Transport in two dimensional electronic micro-emulsions, Ann. Phys. (Amsterdam) **321,** 2071 (2006).

[10] B. Spivak and S. A. Kivelson, Phases intermediate between a two-dimensional electron liquid and Wigner crystal, Phys. Rev. B **70,** 155114 (2004).

[11] L. Radzihovsky and A. Vishwanath, Quantum Liquid Crystals in an Imbalanced Fermi Gas: Fluctuations and Fractional Vortices in Larkin-Ovchinnikov States, Phys. Rev. Lett. **103,** 010404 (2009).

[12] E. Berg, E. Fradkin, and S. A. Kivelson, Charge-4e superconductivity from pair-density-wave order in certain high-temperature superconductors, Nat. Phys. **5,** 830 (2009).

[13] K. Sun, B. M. Fregoso, M. J. Lawler, and E. Fradkin, Fluctuating stripes in strongly correlated electron systems and the nematic-smectic quantum phase transition, Phys. Rev. B **78,** 085124 (2008).

[14] Y. A. Bychkov and E. I. Rashba, Oscillatory effects and the magnetic susceptibility of carriers in inversion layers, J. Phys. C **17,** 6039 (1984).

[15] M. Michiardi, F. Boschini, H.-H. Kung, M. X. Na, S. K. Y. Dufresne, A. Currie, G. Levy, S. Zhdanovich, A. K. Mills, D. J. Jones, J. L. Mi, B. B. Iversen, P. Hofmann, and A. Damascelli, Optical manipulation of Rashba-split 2-dimensional electron gas, Nat. Commun. **13,** 3096 (2022).

[16] K. Wu, J. Chen, H. Ma, L. Wan, W. Hu, and J. Yang, Two-dimensional giant tunable Rashba semiconductors with two-atom-thick buckled honeycomb structure, Nano Lett. **21,** 740 (2021).

[17] Y.-J. Lin, K. Jiménez-García, and I. B. Spielman, Spin-orbit-coupled Bose-Einstein condensates, Nature (London) **471,** 83 (2011).

[18] M. A. Khamehchi, C. Qu, M. E. Mossman, C. Zhang, and P. Engels, Spin-momentum coupled Bose-Einstein condensates with lattice band pseudospins, Nat. Commun. **7,** 10867 (2016).

[19] S.-C. Ji, J.-Y. Zhang, L. Zhang, Z.-D. Du, W. Zheng, Y.-J. Deng, H. Zhai, S. Chen, and J.-W. Pan, Experimental determination of the finite-temperature phase diagram of a spin-orbit coupled Bose gas, Nat. Phys. **10,** 314 (2014).

[20] C. Hamner, Y. Zhang, M. A. Khamehchi, M. J. Davis, and P. Engels, Spin-Orbit-Coupled Bose-Einstein Condensates in a One-Dimensional Optical Lattice, Phys. Rev. Lett. **114,** 070401 (2015).

[21] J.-R. Li, J. Lee, W. Huang, S. Burchesky, B. Shteynas, F. Top, A. O. Jamison, and W. Ketterle, A stripe phase with supersolid properties in spin-orbit-coupled Bose-Einstein condensates, Nature (London) **543,** 91 (2017).

[22] T. M. Bersano, J. Hou, S. Mossman, V. Gokhroo, X.-W. Luo, K. Sun, C. Zhang, and P. Engels, Experimental realization of a long-lived striped Bose-Einstein condensate induced by momentum-space hopping, Phys. Rev. A **99,** 051602(R) (2019).

[23] A. Valdés-Curiel, D. Trypogeorgos, Q.-Y. Liang, R. P. Anderson, and I. B. Spielman, Topological features without a lattice in Rashba spin-orbit coupled atoms, Nat. Commun. **12,** 593 (2021).

[24] S. Sur and K. Yang, Metallic state in bosonic systems with continuously degenerate dispersion minima, Phys. Rev. B **100,** 024519 (2019).

[25] T. A. Sedrakyan, A. Kamenev, and L. I. Glazman, Composite fermion state of spin-orbit-coupled bosons, Phys. Rev. A **86,** 063639 (2012).

[26] R. Liao, Searching for Supersolidity in Ultracold Atomic Bose Condensates with Rashba Spin-Orbit Coupling, Phys. Rev. Lett. **120,** 140403 (2018).

[27] E. Kawasaki and M. Holzmann, Finite-temperature phases of two-dimensional spin-orbit-coupled bosons, Phys. Rev. A **95,** 051601(R) (2017).

[28] S. Sinha, R. Nath, and L. Santos, Trapped Two-Dimensional Condensates with Synthetic Spin-Orbit Coupling, Phys. Rev. Lett. **107,** 270401 (2011).

[29] C.-M. Jian and H. Zhai, Paired superfluidity and fractionalized vortices in systems of spin-orbit coupled bosons, Phys. Rev. B **84,** 060508(R) (2011).

[30] T. Ozawa and G. Baym, Condensation Transition of Ultracold Bose Gases with Rashba Spin-Orbit Coupling, Phys. Rev. Lett. **110,** 085304 (2013).

[31] T. D. Stanescu, B. Anderson, and V. Galitski, Spin-orbit coupled Bose-Einstein condensates, Phys. Rev. A **78,** 023616 (2008).

[32] N. Goldman, G. Juzeliūnas, P. Öhberg, and I. B. Spielman, Light-induced gauge fields for ultracold atoms, Rep. Prog. Phys. **77,** 126401 (2014).

[33] A. L. Fetter and J. D. Walecka, *Quantum Theory of Many-Particle Systems* (Dover Publications, Mineola, New York, 2012).

[34] J. W. Negele and H. Orland, *Quantum Many-Particle Systems* (Perseus Books, New York, 1988).

[35] K. T. Delaney, H. Orland, and G. H. Fredrickson, Numerical Simulation of Finite-Temperature Field Theory for Interacting Bosons, Phys. Rev. Lett. **124,** 070601 (2020).

[36] G. H. Fredrickson and K. T. Delaney, *Field-Theoretic Simulations in Soft Matter and Quantum Fluids*, International Series of Monographs on Physics Vol. 173 (Oxford University Press, Oxford, New York, 2023).

[37] G. Parisi, On complex probabilities, Phys. Lett. **131B,** 393 (1983).

[38] J. R. Klauder, A Langevin approach to fermion and quantum spin correlation functions, J. Phys. A **16,** L317 (1983).

[39] See Supplemental Material at http://link.aps.org/supplemental/10.1103/PhysRevLett.131.173403 for a determination of phase diagram boundaries via superfluid density and grand potential calculations, which includes Refs. [40–42].

[40] S. Mukerjee, C. Xu, and J. E. Moore, Topological Defects and the Superfluid Transition of the $s = 1$ Spinor Condensate in Two Dimensions, Phys. Rev. Lett. **97,** 120406 (2006).

[41] M. Kobayashi, M. Eto, and M. Nitta, Berezinskii-Kosterlitz-Thouless Transition of Two-Component Bose Mixtures with Intercomponent Josephson Coupling, Phys. Rev. Lett. **123,** 075303 (2019).

[42] J. Radić, S. S. Natu, and V. Galitski, Stoner Ferromagnetism in a Thermal Pseudospin-1/2 Bose Gas, Phys. Rev. Lett. **113,** 185302 (2014).

[43] A. L. Subaşı and M. Iskin, Quantum-geometric perspective on spin-orbit-coupled Bose superfluids, Phys. Rev. A **105,** 023301 (2022).

[44] E. G. M. van Kempen, S. J. J. M. F. Kokkelmans, D. J. Heinzen, and B. J. Verhaar, Interisotope Determination of Ultracold Rubidium Interactions from Three High-Precision Experiments, Phys. Rev. Lett. **88,** 093201 (2002).

[45] D. R. Nelson and J. M. Kosterlitz, Universal Jump in the Superfluid Density of Two-Dimensional Superfluids, Phys. Rev. Lett. **39,** 1201 (1977).

[46] J. Toner and D. R. Nelson, Smectic, cholesteric, and Rayleigh-Benard order in two dimensions, Phys. Rev. B **23,** 316 (1981).

[47] M. R. Hammond, E. Cochran, G. H. Fredrickson, and E. J. Kramer, Temperature dependence of order, disorder, and defects in laterally confined diblock copolymer cylinder monolayers, Macromolecules **38,** 6575 (2005).

[48] G. H. Fredrickson and K. T. Delaney, Direct free energy evaluation of classical and quantum many-body systems via field-theoretic simulation, Proc. Natl. Acad. Sci. U.S.A. **119,** e2201804119 (2022).

[49] M. Janoschek, M. Garst, A. Bauer, P. Krautscheid, R. Georgii, P. Böni, and C. Pfleiderer, Fluctuation-induced first-order phase transition in Dzyaloshinskii-Moriya helimagnets, Phys. Rev. B **87,** 134407 (2013).

[50] X.-T. Zhang and G. Chen, Infinite critical boson non-Fermi liquid, npj Quantum Mater. **8,** 10 (2023).

[51] G. Schmid and M. Troyer, Melting of Bosonic Stripes, Phys. Rev. Lett. **93,** 067003 (2004).

[52] C. Hickey and A. Paramekanti, Thermal Phase Transitions of Strongly Correlated Bosons with Spin-Orbit Coupling, Phys. Rev. Lett. **113,** 265302 (2014).

[53] R. Bombín, F. Mazzanti, and J. Boronat, Berezinskii-Kosterlitz-Thouless transition in two-dimensional dipolar stripes, Phys. Rev. A **100,** 063614 (2019).

[54] E. J. Mueller, T.-L. Ho, M. Ueda, and G. Baym, Fragmentation of Bose-Einstein condensates, Phys. Rev. A **74,** 033612 (2006).